This is the accepted manuscript made available via CHORUS. The article has been published as:

Non-Abelian fractional quantum anomalous Hall states and first Landau level physics of the second moiré band of twisted bilayer math xmlns="http://www.w3.org/1998/Math/MathML">msub>mi>MoTe/mi>mn>2/mn>/msub>/math>

Cheong-Eung Ahn, Wonjun Lee, Kunihiro Yananose, Youngwook Kim, and Gil Young Cho

Phys. Rev. B **110**, L161109 — Published 17 October 2024

DOI: 10.1103/PhysRevB.110.L161109

Non-Abelian Fractional Quantum Anomalous Hall States and First Landau Level Physics in Second Moiré Band of Twisted Bilayer $MoTe_2$

Cheong-Eung Ahn,[1,2,*] Wonjun Lee,[1,2,*] Kunihiro Yananose,[3] Youngwook Kim,[4] and Gil Young Cho[1,2,5,†]

[1] *Department of Physics, Pohang University of Science and Technology, Pohang, 37673, Republic of Korea*
[2] *Center for Artificial Low Dimensional Electronic Systems, Institute for Basic Science, Pohang 37673, Korea*
[3] *Korea Institute for Advanced Study, Seoul 02455, Korea*
[4] *Department of Physics and Chemistry, Daegu Gyeongbuk Institute of Science and Technology (DGIST), Daegu 42988, Republic of Korea*
[5] *Asia-Pacific Center for Theoretical Physics, Pohang, Gyeongbuk, 37673, Korea*

(Dated: August 19, 2024)

Utilizing the realistic continuum description of twisted bilayer $MoTe_2$ and many-body exact diagonalization calculation, we establish that the second moiré band of twisted bilayer MoTe2, at a small twist angle of approximately 2°, serves as an optimal platform for achieving the long-sought non-Abelian fractional quantum anomalous Hall states without the need for external magnetic fields. Across a wide parameter range, our exact diagonalization calculations reveal that the half-filled second moiré band demonstrates the ground state degeneracy and spectral flows, which are consistent with the pfaffian state in the first Landau level. We further elucidate that the emergence of the non-Abelian state is deeply connected to the remarkable similarity between the second moiré band and the first Landau level. Essentially, the band not only exhibits characteristics akin to the first Landau level, $\frac{1}{2\pi}\int_{\mathrm{BZ}} \mathrm{d}^2\mathbf{k}\ \mathrm{tr}\,\eta(\mathbf{k}) \approx 3$ where $\eta_{ab}(\mathbf{k})$ is the Fubini-Study metric of the band, but also that its projected Coulomb interaction closely mirrors the Haldane pseudopotentials of the first Landau level. Motivated from this observation, we introduce a novel metric of "first Landau level"-ness of a band, which quantitatively measures the alignment of the projected Coulomb interaction with the Haldane pseudopotentials in Landau levels. This metric is then compared with the global phase diagram of the half-filled second moire band, revealing its utility in predicting the parameter region of the non-Abelian state. In addition, we uncover that the first and third moiré bands closely resemble the lowest and second Landau levels, revealing a remarkable sequential equivalence between the moiré bands and Landau levels. We finally discuss the potential implications on experiments.

Twisted moiré materials have unveiled various exciting quantum phenomena, encompassing Mott insulators [1, 2], strange metals [3], and superconductivity [4, 5]. Even more surprisingly, recent transport experiments on twisted $MoTe_2$ ($tMoTe_2$) and pentalayer graphene systems uncovered the emergence of fractional quantum anomalous Hall states (FQAH) and composite Fermi liquids at zero external magnetic fields [6–11], which strikingly parallels the physics of quantum Hall states under large magnetic fields in the lowest Landau levels. While the discovery of the FQAH in experiments is interesting, it is noteworthy that the states observed to date align with the Abelian quantum Hall states [12–20], which only accommodate the Abelian anyons. On the other hand, the anomalous version of non-Abelian fractional quantum Hall states in the first Landau level, which could lay the practical groundwork for the fault-tolerant topological quantum computer and thus have immense importance [21], remains undiscovered.

In this Letter, we demonstrate that the *second* moiré band of $tMoTe_2$ around the twist angle $\theta \sim 2°$ is an ideal platform for the realization of this long-sought non-Abelian FQAHs. This is in a sharp contrast to the previous research, which has focused on the *first* moiré band of $tMoTe_2$ at *larger twist angles* $\theta \sim 4°$ [15–20]. Our analysis is based on the continuum description of the density functional theory (DFT) band structure [22] and many-body exact diagonalization calculation (ED). Our ED calculation finds that when half-filled, the second moiré band gives rise to the ground state degeneracy, which is consistent with the putative non-Abelian fractional quantum Hall states in the first Landau level, i.e., pfaffian state [23]. Notably, $tMoTe_2$ and twisted bilayer WSe_2 with the small twist angles are readily available in experiments [11, 24], which calls for further experiments.

Interestingly, we find that behind the emergence of the non-Abelian FQAHs, the striking resemblance of of the second moiré band and the first Landau level (1LL) exists. This contrasts with the first moiré band of $tMoTe_2$ for $\theta \gtrsim 3.9°$, which is widely recognized for its resemblance to the lowest Landau Level (LLL) [17–20, 25–28]. Essentially, we observe that the projected Coulomb interaction closely mirrors the Haldane pseudopotential in 1LL while the band fulfills the known 1LL trace condition $\frac{1}{2\pi}\int_{\mathrm{BZ}} \mathrm{d}^2\mathbf{k}\ \mathrm{tr}\,\eta(\mathbf{k}) \approx 3$, where $\eta_{ab}(\mathbf{k}) = \mathrm{Re}\{\langle\partial_{k_a} u(\mathbf{k})|(\mathbb{I} - |u(\mathbf{k})\rangle\langle u(\mathbf{k})|)|\partial_{k_b} u(\mathbf{k})\rangle\}$ is the Fubini-Study metric of the Bloch function $|u(\mathbf{k})\rangle$ [29, 30]. These two conditions are in principle independent to each other, however should both be satisfied to best mimic the physics of 1LL. Motivated by this observation, we present a new metric Eq.(2) for 1LL-ness of the band, which quantifies the similarity of the projected Coulomb inter-

angle	v_1	ψ	γ_1	v_2	γ_2	Ref.
$\gg 1^\circ$	8	-89.6°	-8.5	0	0	[33]
4.4°	11.2	-91°	-13.3	0	0	[14]
3.9°	7.5	-100°	-11.3	0	0	[14]
-	9.2	-99°	-11.2	0	0	[18]
-	20.8	-107.7°	-23.8	0	0	[15]
-	17.0	-107.7°	-16.0	0	0	[34]
-	16.5	-105.9°	-18.8	0	0	[27]
-	7.94	-88.43°	-10.77	20.00	10.21	[27]
-	9.45	-85.23°	-12.20	24.99	13.12	[22, 35]
2.1°	20.51	-61.49°	-7.01	-9.08	11.08	[22, 35]

TABLE I: **Continuum model parameters.** The parameters v_1, γ_1, v_2, γ_2 are given in units of meV.

action to the Haldane pseudopotentials in 1LL. Notably, the full characterization of the 1LL-like Chern bands is currently a subject of active research [29, 30]. Our metric could offer a valuable and quantitative tool for this purpose, with wide applicability. Finally, we also compare the global phase diagram around the FQAH and the values of our new metric, revealing its utility in predicting the parameter region of the 1LL-ness.

Before proceeding further, let us compare our findings with the existing studies. First, [31] explored the first moiré band of $tMoTe_2$ at $\theta \sim 3.9^\circ$ with three-body interactions. On the other hand, [32] investigated a skyrmion Chern band model, which captures the essence of twisted bilayer transition metal dichalcogenides. Within this model, [32] also pointed out the 1LL-like nature of the second moiré band and emergence of the non-Abelian FQAH, using the wavefunction overlap of the single-hole states in their model with corresponding 1LL states. Our work distinguishes itself by focusing directly on the second moiré band of a realistic continuum model near $\theta \sim 2^\circ$ and revealing 1LL-ness through the projected Coulomb interactions.

1. Continuum Model. We start with the continuum model [33] of $tMoTe_2$ around the K-valley (with $\hbar = 1$)

$$\hat{h}_\uparrow = \begin{bmatrix} -\frac{(\hat{\mathbf{k}}-K_+)^2}{2m^*} + V_+(\hat{\mathbf{r}}) & \Gamma^*(\hat{\mathbf{r}}) \\ \Gamma(\hat{\mathbf{r}}) & -\frac{(\hat{\mathbf{k}}-K_-)^2}{2m^*} + V_-(\hat{\mathbf{r}}) \end{bmatrix}, \quad (1)$$

where m^* is the effective mass of the monolayer electron, $K_\pm = R_{\pm\theta/2}K$ are the twisted K points of the top and bottom layers, $V_\pm(\mathbf{r})$ and $\Gamma(\mathbf{r})$ are the intralayer and interlayer moiré potentials, respectively. The Hamiltonian around the $(-K)$-valley is the time-reversal conjugate of Eq.(1). There have been several DFT studies on $tMoTe_2$ at various twist angles [14, 15, 18, 22, 27, 34, 36]. For our focus, i.e., $tMoTe_2$ near $\theta \sim 2.1^\circ$, we find the parameters $(v_1, \psi, \gamma_1, v_2, \gamma_2)$ of the moiré potentials by fitting the band structure of Eq.(1) to that in [22] along the high-symmetry lines in momentum space [35], up to valley-reduced inversion symmetric second harmonics [27, 35, 36]. The resulting parameters are listed in Table I, whose band structure is in [Fig.1(a)].

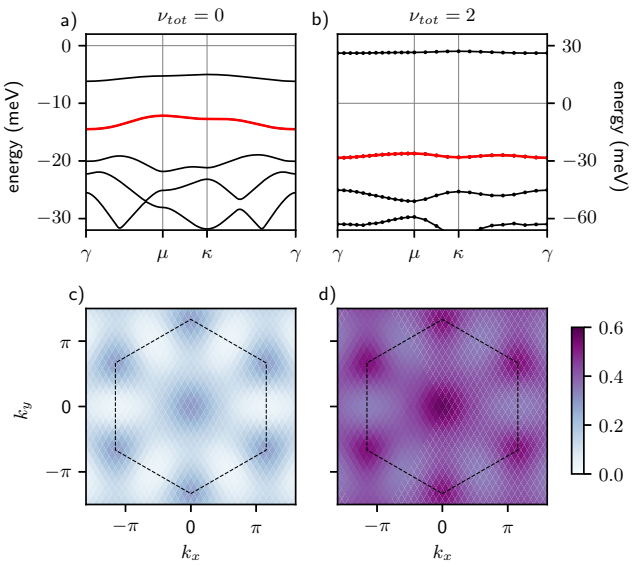


FIG. 1: (a) Band structure at $\nu_h = 0$ and (b) its SCHF-corrected band structure at $\nu_h = 2$ with $\epsilon_r = 5.0$. (c) Berry curvature and (d) trace of the Fubini-Study metric of the SCHF-corrected second moiré band. The black dashed line represents the moiré BZ with $a_M = 1$.

A few comments are in order. First, we confirmed that the model parameters for $\theta \sim 2^\circ$ produces the series of the valley Chern numbers, consistent with the DFT calculation [22] and also the experiment [11]. This supports the validity of our continuum model Eq.(1) beyond the numerical fitting. Specifically, each of the three moiré bands ($a = 1, 2, 3$) exhibit a valley-projected Chern number of $C_{\uparrow,a} = +1$ with $C_{\uparrow,a} = -C_{\downarrow,a}$. Secondly, from Table I, we observe a significant renormalization of the model parameters for $\theta \sim 2.1^\circ$ relative to those for $\theta \gtrsim 3.9^\circ$ [14, 15, 18, 22, 27, 33, 34]. As discussed in [22, 27, 36], the higher harmonics in the model parameters are expected to play a significant role at smaller twist angles, and they can even undergo a rapid change in sign with twist angle. This is reflected in the sign of v_2 for $\theta \sim 2.1^\circ$ relative to those for $\theta \gtrsim 3.9^\circ$. Despite of these drastic differences in model parameters, the moiré band widths at $\theta \sim 2.1^\circ$ remain small, approximately 2.4 meV, signifying the importance of the interactions.

2. Coulomb Interaction. We assume the Coulomb interaction [12–20]

$$H = -\hat{h} + \frac{1}{2A}\sum_{\mathbf{p}} V_{\mathbf{p}} :\hat{\rho}_{\mathbf{p}}\hat{\rho}_{-\mathbf{p}}:$$

Here, $\hat{\rho}_{\mathbf{p}} = \sum_{\tau,\mathbf{k},\ell} \hat{c}^\dagger_{\tau,\mathbf{k}+\mathbf{p},\ell}\hat{c}_{\tau,\mathbf{k},\ell}$ is the density operator, A is the sample area, and the normal ordering is against $\nu_h = 0$, and

$$V_{\mathbf{p}} = \left(\frac{e^2}{4\pi\epsilon_0}\right)\left(2\pi\epsilon_r^{-1}\right)\frac{\tanh(p\xi/2)}{p},$$

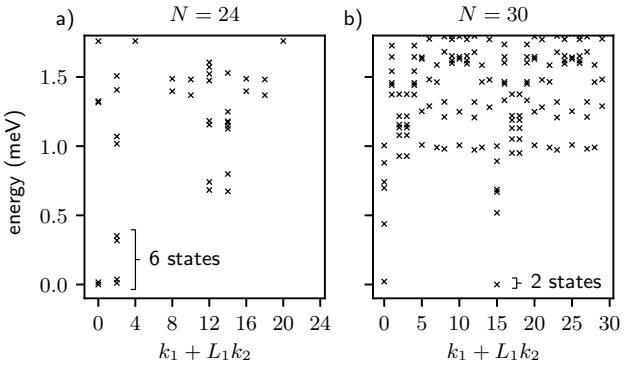


FIG. 2: Energy spectrum on a torus of (a) 4×6, and (b) 5×6 unitcells.

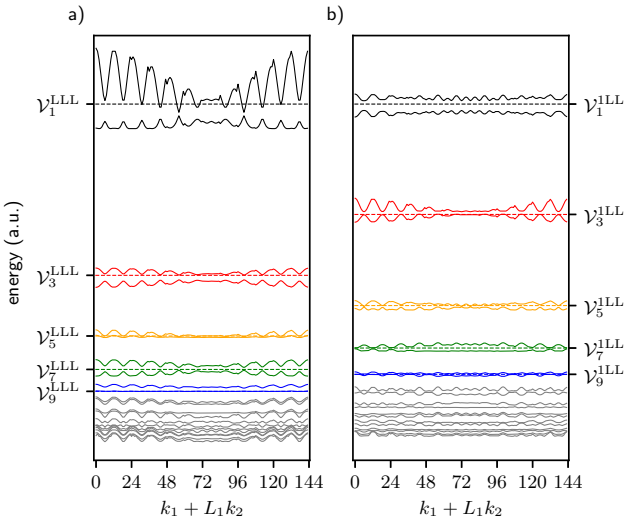


FIG. 3: Effective Haldane pseudopotentials of projected Coulomb interactions. The solid lines are the estimated Haldane pseudopotential of (a) the first moiré band at $\theta = 3.7°$ and (b) the second moiré band at $\theta = 2.1°$ on a torus of 12×12 unitcells. In both cases, we take $\epsilon_r = 5$. The dashed lines are the exact Haldane pseudopotentials of (a) LLL and (b) 1LL.

where ξ is the gate distance and ϵ_r is the relative permittivity. For simplicity, we set $\xi = \infty$, i.e., the unscreened Coulomb interaction, as its precise value has little effect on FQAHs due to the large size of the moiré unitcell [19].

As the DFT band is obtained at $\nu_h = 0$, we use the self-consistent Hartree-Fock (SCHF) method to obtain the renormalized second moiré band at $\nu_h = 2$, its Berry curvature and trace of the Fubini-Study metric [Fig.1(b-d)]. The Hartree-Fock correction makes the Berry curvature and trace of the Fubini-Study metric significantly more uniform, similar to the valley-polarized first moiré band at $\nu_h = 1$ [14, 17, 19]. Some details on SCHF can be found in [35]. On the other hand, the trace of the Fubini-Study metric, i.e., $\mathrm{tr}\,\eta(\mathbf{k})$, is much larger than the absolute Berry curvature, suggesting that the second moiré band is distinct from LLL-like bands [37–39]. Indeed, the quantum weight $\frac{1}{2\pi}\int_{\mathrm{BZ}} \mathrm{d}^2\mathbf{k}\,\mathrm{tr}\,\eta(\mathbf{k})$ for $\epsilon_r = 5$ reaches 3.04 approximately, well satisfying a property of 1LL-like bands [29, 30], whereas the Chern number is $C = 1$. We note that while a mathematically precise criteria for 1LL-like bands has recently been proposed in [30], it requires the global information of band structures. Hence, a direct characterization of 1LL-like bands from local quantum geometry has yet to be found, as noted in [30].

3. Non-Abelian FQAH. Driven by the resemblance of the second moiré bands to 1LL, we undertake ED calculations to search for a non-Abelian FQAH state. Our analysis focuses on a half-filled, SCHF-corrected second moiré band. We first find that, for a system of 3×4 unitcells, the ground state is fully valley-polarized for a wide range of twist angles $\theta \in [1.5°, 3.0°]$ and dielectric constants $\epsilon_r \in [2, 10]$ under the assumption that all model parameters in Eq.(1) remain unchanged except θ [35]. This robust valley polarization mirrors that observed in the first moiré band within the Coulomb and dual-gate screened Coulomb interaction [12, 14, 15, 19, 40]. Building on this, we next narrow our ED investigation to a single valley.

In [Fig.2(a,b)], we present the many-body energy spectra of a single valley for 4×6 and 5×6 unitcells at $\epsilon_r = 5.0$ and $\theta = 2.1°$. Importantly, we observe the emergence of six-fold and two-fold degenerate ground states for even and odd number of holes, matching precisely those of the pfaffian state [23, 41], which strongly suggests the emergence of a non-Abelian FQAH. In [35], we report the spectral flow and additional energy spectrum, which further support the emergence of the pfaffian state.

4. 1LL-like Projected Interactions. While FQAHs require both the appropriate band structure and interactions, much of the previous literature [14, 17, 19, 25–27, 32, 42–44] focuses largely on the band characteristics like the Fubini-Study metric to discuss the nLL-ness. Here, we focus on the nature of the projected Coulomb interaction in moiré bands and compare them with those in LLs.

To have a fair comparison of the projected Coulomb interaction in the second moiré band with that in 1LL, we calculate the effective Haldane pseudopoentials of the projected interaction from the energy spectrum of two holes [45]. When the band is completely flat and the projected interaction respects the translation symmetry, the energy levels of the two holes are expected to organize into pairs, irrespective of momentum. Then, the first highest pair's energy is $\mathcal{V}_1$, the second pair's energy is $\mathcal{V}_3$, the third pair's is $\mathcal{V}_5$, and so forth. If the band under consideration perfectly mimics the physics of the nLL, one expects that the pseudopotential obtained

in this way will be equal to those of the nLL projected Coulomb interaction, namely the Haldane pseudopotentials $\mathcal{V}_\ell^{n\mathrm{LL}}$ ($\ell = 1, 3, 5, \cdots$), up to a global scale. For non-ideal bands, the pairs are split and show momentum dependence.

Spectacularly, we observe that the effective Haldane pseudopotentials of the projected Coulomb interaction in the SCHF-renormalized second moiré band at $\theta \sim 2.1°$ [Fig.1(b)] is close to those of the 1LL-projected Coulomb interaction [Fig.3(b)]. This provides further support of the emergence of the 1LL-like non-Abelian FQAH in our ED calculation. Following the same calculation, we can also demonstrate that for the first moiré band at $\theta = 3.7°$, the effective pseudopotential of the projected Coulomb interaction is similar to the Haldane pseudopotential in LLL [Fig.3(a)], consistent with previous characterization of the first moiré band in terms of quantum geometry [14, 17, 19, 25–27]. For the latter, we used the continuum model Eq.(1) with model parameters for $\theta \sim 3.9°$ [22, 35], also reported in Table.I.

By investigating the projected interactions and quantum weight, we uncover that the other moiré bands at $\theta \sim 2.1°$ also closely resembles the physics of the corresponding Landau levels [35] as like the second moiré band resembles 1LL. More precisely, the effective Haldane pseudopotentials and the quantum weight $\frac{1}{2\pi}\int_{\mathrm{BZ}} \mathrm{d}^2\mathbf{k}\ \mathrm{tr}\,\eta(\mathbf{k})$ of the third moiré band are close to those of 2LL, and those of the first moiré band are close to those of LLL. Detailed calculations and consequences of the above can be found in [35]. Hence, in $tMoTe_2$ at $\theta \sim 2.1°$, we remarkably find that the physics of the moiré bands sequentially matches those of the Landau levels.

Motivated by the similarity of the projected interaction to the Haldane pseudopotentials, we propose a quantitative metric for the nLL-ness

$$S^2 = \frac{1}{N}\sum_{\mathbf{K}}\sum_{m=1}^{\infty} w_{2m-1}\left(\left|\frac{\tilde{E}_{\mathbf{K},2m-1}-E_0}{E_1-E_0} - \frac{v_{2m-1}^{n\mathrm{LL}}}{v_1^{n\mathrm{LL}}}\right|^2 + \left|\frac{\tilde{E}_{\mathbf{K},2m}-E_0}{E_1-E_0} - \frac{v_{2m-1}^{n\mathrm{LL}}}{v_1^{n\mathrm{LL}}}\right|^2\right) \geq 0, \qquad (2)$$

where $\tilde{E}_{\mathbf{K},a}$ ($a = 1, 2, 3, \cdots$) are the energy levels of the total momentum sector $\mathbf{K} = \mathbf{k}_1 + \mathbf{k}_2$ of the two holes in *descending* order, and E_1, E_0 are the global scaling factors. Each ℓ-th term in the sum is weighted by $w_\ell \in [0, 1]$. To correctly capture the similarity to the Landau levels, we need to set the first few weights large while $w_\ell \to 0$ for large enough ℓ. A more detailed discussion can be found in [35]. This metric measures both the deviation of the estimated pseudopotentials from those of nLL, and also the non-ideality of the band like the non-flatness and non-uniform quantum geometry. The smaller the metric S is, the projected interaction to the band is closer to the Haldane pseudopotential in nLL.

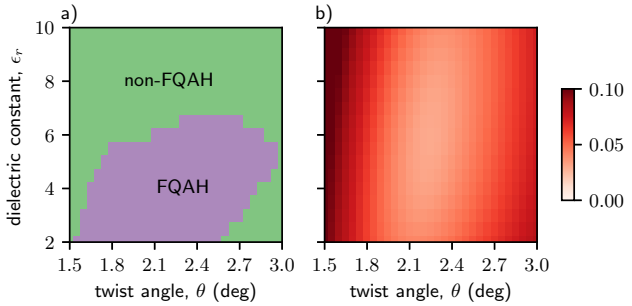


FIG. 4: (a) Phase diagram. (b) Value of 1LL-ness S, Eq.(2) for $w_\ell = 1$ for $\ell \leq 9$ and $w_\ell = 0$ for $\ell > 9$.

Below, we will compare its value with the many-body phase diagram.

We leave a few important remarks on Eq.(2). First, the computation of S is much less costly than ED, because it requires the energy spectrum for just two particles. When N is the number of unitcells, the cost is $\sim N^3$. Secondly, given that the projected Coulomb interaction does depend on the band characteristics, the comparison of the effective Haldane pseudopotential with those of the nLL can provide a useful alternative metric for the nLL-ness of Chern bands.

5. Phase Diagram. Within ED, we draw the many-body phase diagram over the parameter space of $\theta \in [1.5°, 3.0°]$ and $\epsilon_r \in [2, 10]$, while holding other model parameters in Eq.(1) invariant. Over this parameter space, we have confirmed that the system is fully valley polarized [35], and thus we perform ED on a single valley for $N = 4 \times 6$ unitcells. Our primary focus is to identify the non-Abelian FQAH, whose lowest energy levels are in one-to-one correspondence with those in 1LL [32]. The resulting phase diagram is in [Fig.4(a)], which is compared with the value of S Eq.(2). We observe that the projected interaction in the second moiré band remains close to the projected Coulomb interaction in 1LL for a wide range of angles and interaction strengths, with an optimal value in the vicinity of $\theta \sim 2.2°$ and $\epsilon_r \sim 6$ [Fig.4(b)]. Globally, we find that the FQAH state is stabilized when the interaction strength is large enough, and when the projected interaction is 1LL-like, i.e., S is small enough, revealing the efficacy of our metric Eq.(2).

6. Conclusions. We have shown that the behavior of the second moiré band in $tMoTe_2$ around $\theta \sim 2.1°$ exhibits remarkable parallels with 1LL. This similarity is not just limited to the band's characteristics $\frac{1}{2\pi}\int_{\mathrm{BZ}} \mathrm{d}^2\mathbf{k}\ \mathrm{tr}\,\eta(\mathbf{k}) \approx 3$, but also extends to the nature of the projected Coulomb interaction, which closely resembles the Haldane pseudopotentials in 1LL. These observations collectively hint at the possible emergence of a non-Abelian FQAH at $\nu_h = 2 + 1/2$, which we have confirmed through ED calculations. Moreover, we introduced a novel metric Eq.(2) of 1LL-ness of a band, which

measures the similarity between the projected Coulomb interaction and the Haldane pseudopotentials in 1LL. This new metric S agrees reasonably well with the region where the FQAH is stabilized [Fig.4], when the interaction is strong enough.

Finally, our theory here clearly demonstrates that the $tMoTe_2$ or twisted bilayer WSe_2 with small twist angles [11, 24] represent a promising path for the 1LL-like non-Abelian FQAHs. In particular, in these two-dimensional moire materials, there are various tuning parameters like displacement field, interlayer distance via pressure, and substrate variations, which may lead to the eagerly-anticipated discovery of the 1LL-like non-Abelian FQAHs.

- *Note Added*: Near the completion of this work, we became aware of the two similar works [32, 46]. An updated version (v2) of [32] identified a non-Abelian FQAH in the second moiré band of a skyrmion Chern band model, which is adiabatically-connected to the continuum model of twisted bilayer $MoTe_2$ at $\theta \sim 2.5°$, while [46] identified a non-Abelian FQAH in the second moiré band of the continuum model over a wide range of twist angles, using the parameters fitted to their DFT calculations of twisted bilayer $MoTe_2$ at $\theta \sim 1.9°$.

We thank Yong Baek Kim and Kwon Park for helpful discussions and Young-Woo Son for collaborations in related works. C.-E. A., W. L. and G.Y.C. are supported by Samsung Science and Technology Foundation under Project Number SSTF-BA2002-05 and SSTF-BA2401-03, the NRF of Korea (Grant No.RS-2023-00208291, No.2023M3K5A1094810, No.2023M3K5A1094813, No.RS-2024-00410027, No. RS-2024-00444725) funded by the Korean Government (MSIT), the Air Force Office of Scientific Research under Award No.FA2386-22-1-4061, and Institute of Basic Science under project code IBS-R014-D1. K. Y. was supported by a KIAS individual grant (CG092501) at Korea Institute for Advanced Study. A part of computations were supported by Center for Advanced Computation of KIAS. Y. K. is supported by NRF of Korea (2020R1C1C1006914, 2022M3H3A1098408) funded by the Korean Government (MSIT).

* These authors contributed equally.
† gilyoungcho@postech.ac.kr

[1] Y. Cao, V. Fatemi, A. Demir, S. Fang, S. L. Tomarken, J. Y. Luo, J. D. Sanchez-Yamagishi, K. Watanabe, T. Taniguchi, E. Kaxiras, et al., Correlated insulator behaviour at half-filling in magic-angle graphene superlattices, Nature **556**, 80 (2018).
[2] E. C. Regan, D. Wang, C. Jin, M. I. Bakti Utama, B. Gao, X. Wei, S. Zhao, W. Zhao, Z. Zhang, K. Yumigeta, et al., Mott and generalized Wigner crystal states in WSe_2/WS_2 moiré superlattices, Nature **579**, 359 (2020).
[3] Y. Cao, D. Chowdhury, D. Rodan-Legrain, O. Rubies-Bigorda, K. Watanabe, T. Taniguchi, T. Senthil, and P. Jarillo-Herrero, Strange metal in magic-angle graphene with near Planckian dissipation, Physical review letters **124**, 076801 (2020).
[4] Y. Cao, V. Fatemi, S. Fang, K. Watanabe, T. Taniguchi, E. Kaxiras, and P. Jarillo-Herrero, Unconventional superconductivity in magic-angle graphene superlattices, Nature **556**, 43 (2018).
[5] G. Chen, A. L. Sharpe, P. Gallagher, I. T. Rosen, E. J. Fox, L. Jiang, B. Lyu, H. Li, K. Watanabe, T. Taniguchi, et al., Signatures of tunable superconductivity in a trilayer graphene moiré superlattice, Nature **572**, 215 (2019).
[6] J. Cai, E. Anderson, C. Wang, X. Zhang, X. Liu, W. Holtzmann, Y. Zhang, F. Fan, T. Taniguchi, K. Watanabe, et al., Signatures of fractional quantum anomalous Hall states in twisted $MoTe_2$, Nature **622**, 63 (2023).
[7] Y. Zeng, Z. Xia, K. Kang, J. Zhu, P. Knüppel, C. Vaswani, K. Watanabe, T. Taniguchi, K. F. Mak, and J. Shan, Thermodynamic evidence of fractional Chern insulator in moiré $MoTe_2$, Nature **622**, 69 (2023).
[8] H. Park, J. Cai, E. Anderson, Y. Zhang, J. Zhu, X. Liu, C. Wang, W. Holtzmann, C. Hu, Z. Liu, et al., Observation of fractionally quantized anomalous Hall effect, Nature **622**, 74 (2023).
[9] F. Xu, Z. Sun, T. Jia, C. Liu, C. Xu, C. Li, Y. Gu, K. Watanabe, T. Taniguchi, B. Tong, et al., Observation of integer and fractional quantum anomalous Hall effects in twisted bilayer $MoTe_2$, Physical Review X **13**, 031037 (2023).
[10] Z. Lu, T. Han, Y. Yao, A. P. Reddy, J. Yang, J. Seo, K. Watanabe, T. Taniguchi, L. Fu, and L. Ju, Fractional quantum anomalous Hall effect in multilayer graphene, Nature **626**, 759 (2024).
[11] K. Kang, B. Shen, Y. Qiu, Y. Zeng, Z. Xia, K. Watanabe, T. Taniguchi, J. Shan, and K. F. Mak, Evidence of the fractional quantum spin Hall effect in moiré $MoTe_2$, Nature **628**, 522 (2024).
[12] H. Li, U. Kumar, K. Sun, and S.-Z. Lin, Spontaneous fractional Chern insulators in transition metal dichalcogenide moiré superlattices, Physical Review Research **3**, L032070 (2021).
[13] V. Crépel and L. Fu, Anomalous Hall metal and fractional Chern insulator in twisted transition metal dichalcogenides, Physical Review B **107**, L201109 (2023).
[14] A. P. Reddy, F. Alsallom, Y. Zhang, T. Devakul, and L. Fu, Fractional quantum anomalous Hall states in twisted bilayer $MoTe_2$ and WSe_2, Physical Review B **108**, 085117 (2023).
[15] C. Wang, X.-W. Zhang, X. Liu, Y. He, X. Xu, Y. Ran, T. Cao, and D. Xiao, Fractional Chern insulator in twisted bilayer $MoTe_2$, Physical Review Letters **132**, 036501 (2024).
[16] A. Abouelkomsan, A. P. Reddy, L. Fu, and E. J. Bergholtz, Band mixing in the quantum anomalous Hall regime of twisted semiconductor bilayers, Physical Review B **109**, L121107 (2024).
[17] J. Dong, J. Wang, P. J. Ledwith, A. Vishwanath, and D. E. Parker, Composite fermi liquid at zero magnetic

field in twisted $MoTe_2$, Physical Review Letters **131**, 136502 (2023).
[18] C. Xu, J. Li, Y. Xu, Z. Bi, and Y. Zhang, Maximally localized Wannier functions, interaction models, and fractional quantum anomalous Hall effect in twisted bilayer $MoTe_2$, Proceedings of the National Academy of Sciences **121**, e2316749121 (2024).
[19] J. Yu, J. Herzog-Arbeitman, M. Wang, O. Vafek, B. A. Bernevig, and N. Regnault, Fractional Chern insulators versus nonmagnetic states in twisted bilayer $MoTe_2$, Physical Review B **109**, 045147 (2024).
[20] A. P. Reddy and L. Fu, Toward a global phase diagram of the fractional quantum anomalous Hall effect, Physical Review B **108**, 245159 (2023).
[21] C. Nayak, S. H. Simon, A. Stern, M. Freedman, and S. D. Sarma, Non-abelian anyons and topological quantum computation, Reviews of Modern Physics **80**, 1083 (2008).
[22] X.-W. Zhang, C. Wang, X. Liu, Y. Fan, T. Cao, and D. Xiao, Polarization-driven band topology evolution in twisted $MoTe_2$ and WSe_2, Nature Communications **15**, 4223 (2024).
[23] N. Read and D. Green, Paired states of fermions in two dimensions with breaking of parity and time-reversal symmetries and the fractional quantum Hall effect, Physical Review B **61**, 10267 (2000).
[24] K. Kang, Y. Qiu, K. Watanabe, T. Taniguchi, J. Shan, and K. F. Mak, Observation of the double quantum spin Hall phase in moiré WSe_2, arXiv preprint arXiv:2402.04196 (2024).
[25] T. Devakul, V. Crépel, Y. Zhang, and L. Fu, Magic in twisted transition metal dichalcogenide bilayers, Nature communications **12**, 6730 (2021).
[26] N. Morales-Durán, N. Wei, J. Shi, and A. H. MacDonald, Magic angles and fractional Chern insulators in twisted homobilayer transition metal dichalcogenides, Physical Review Letters **132**, 096602 (2024).
[27] Y. Jia, J. Yu, J. Liu, J. Herzog-Arbeitman, Z. Qi, H. Pi, N. Regnault, H. Weng, B. A. Bernevig, and Q. Wu, Moiré fractional Chern insulators. I. first-principles calculations and continuum models of twisted bilayer $MoTe_2$, Physical Review B **109**, 205121 (2024).
[28] V. Crépel, N. Regnault, and R. Queiroz, Chiral limit and origin of topological flat bands in twisted transition metal dichalcogenide homobilayers, Communications Physics **7**, 146 (2024).
[29] T. Ozawa and B. Mera, Relations between topology and the quantum metric for Chern insulators, Physical Review B **104**, 045103 (2021).
[30] M. Fujimoto, D. E. Parker, J. Dong, E. Khalaf, A. Vishwanath, and P. Ledwith, Higher vortexability: zero field realization of higher Landau levels, arXiv preprint arXiv:2403.00856 (2024).
[31] L. Zhang and X.-Y. Song, Moore-Read state in half-filled moiré Chern band from three-body pseudo-potential, arXiv preprint arXiv:2403.11478 (2024).
[32] A. P. Reddy, N. Paul, A. Abouelkomsan, and L. Fu, Non-abelian fractionalization in topological minibands, arXiv preprint arXiv:2403.00059 (2024).
[33] F. Wu, T. Lovorn, E. Tutuc, I. Martin, and A. MacDonald, Topological insulators in twisted transition metal dichalcogenide homobilayers, Physical review letters **122**, 086402 (2019).
[34] T. Wang, M. Wang, W. Kim, S. G. Louie, L. Fu, and M. P. Zaletel, Topology, magnetism and charge order in twisted $MoTe_2$ at higher integer hole fillings, arXiv preprint arXiv:2312.12531 (2023).
[35] See Supplemental Material at https://journals.aps.org/prb/, which includes Refs.[47–55], for detailed discussion of previous experiments, numerical simulation methodology, and our results.
[36] N. Mao, C. Xu, J. Li, T. Bao, P. Liu, Y. Xu, C. Felser, L. Fu, and Y. Zhang, Transfer learning relaxation, electronic structure and continuum model for twisted bilayer $MoTe_2$, Communications Physics **7**, 262 (2024).
[37] S. Parameswaran, R. Roy, and S. L. Sondhi, Fractional Chern insulators and the W_∞ algebra, Physical Review B **85**, 241308 (2012).
[38] S. A. Parameswaran, R. Roy, and S. L. Sondhi, Fractional quantum Hall physics in topological flat bands, Comptes Rendus Physique **14**, 816 (2013).
[39] P. J. Ledwith, A. Vishwanath, and D. E. Parker, Vortexability: A unifying criterion for ideal fractional Chern insulators, Physical Review B **108**, 205144 (2023).
[40] P. Potasz, N. Morales-Durán, N. C. Hu, and A. H. MacDonald, Itinerant ferromagnetism in transition metal dichalcogenide moiré superlattices, Physical Review B **109**, 045144 (2024).
[41] M. Oshikawa, Y. B. Kim, K. Shtengel, C. Nayak, and S. Tewari, Topological degeneracy of non-abelian states for dummies, Annals of Physics **322**, 1477 (2007).
[42] J. Wang, J. Cano, A. J. Millis, Z. Liu, and B. Yang, Exact Landau level description of geometry and interaction in a flatband, Physical review letters **127**, 246403 (2021).
[43] J. Wang and Z. Liu, Hierarchy of ideal flatbands in chiral twisted multilayer graphene models, Physical Review Letters **128**, 176403 (2022).
[44] J. Wang, S. Klevtsov, and Z. Liu, Origin of model fractional Chern insulators in all topological ideal flatbands: Explicit color-entangled wave function and exact density algebra, Physical Review Research **5**, 023167 (2023).
[45] A. M. Läuchli, Z. Liu, E. J. Bergholtz, and R. Moessner, Hierarchy of fractional Chern insulators and competing compressible states, Physical Review Letters **111**, 126802 (2013).
[46] C. Xu, N. Mao, T. Zeng, and Y. Zhang, Multiple Chern bands in twisted $MoTe_2$ and possible non-abelian states, arXiv preprint arXiv:2403.17003 (2024).
[47] E. Cancès and C. Le Bris, Can we outperform the diis approach for electronic structure calculations?, International Journal of Quantum Chemistry **79**, 82 (2000).
[48] A. J. Cohen, P. Mori-Sánchez, and W. Yang, Insights into current limitations of density functional theory, Science **321**, 792 (2008).
[49] T. Brumme, M. Calandra, and F. Mauri, Electrochemical doping of few-layer ZrNCl from first principles: Electronic and structural properties in field-effect configuration, Physical Review B **89**, 245406 (2014).
[50] J.-H. Lee and Y.-W. Son, Gate-tunable superconductivity and charge-density wave in monolayer $1T'$-$MoTe_2$ and $1T'$-WTe_2, Physical Chemistry Chemical Physics **23**, 17279 (2021).
[51] Z. Liu and E. J. Bergholtz, From fractional Chern insulators to abelian and non-abelian fractional quantum Hall states: Adiabatic continuity and orbital entanglement spectrum, Physical Review B **87**, 035306 (2013).
[52] D. Wang, Z. Liu, W.-M. Liu, J. Cao, and H. Fan,

Fermionic non-abelian fractional Chern insulators from dipolar interactions, Physical Review B **91**, 125138 (2015).

[53] M. R. Peterson, T. Jolicoeur, and S. Das Sarma, Orbital Landau level dependence of the fractional quantum Hall effect in quasi-two-dimensional electron layers: Finite-thickness effects, Physical Review B **78**, 155308 (2008).

[54] M. P. Zaletel, R. S. Mong, and F. Pollmann, Topological characterization of fractional quantum Hall ground states from microscopic Hamiltonians, Physical review letters **110**, 236801 (2013).

[55] D. Tong, Lectures on the quantum Hall effect, arXiv preprint arXiv:1606.06687 (2016).